A High-Efficiency, Simple-Structure, Compact Wideband Microwave Energy Harvester for Wirelessly Powered IoT Receivers

Jiupei Shi, *Student Member, IEEE*, Chaoyun Song, *Senior Member, IEEE*, Yejun He, *Senior Member, IEEE*, Cheng Zhang, *Member, IEEE*, Yuchao Wang, Zhonghe Zhang, Jinyao Zhang, Wenting Li, *Member, IEEE*, and Yi Huang, *Fellow, IEEE*

***Abstract*—Wireless data links and wireless power transfer (WPT) have become emerging topics in IoT applications. A simple-structure high-efficiency rectenna is the key technology for wirelessly powered IoT receivers. Herein, we explore a unified co-design technique that synergizes wideband circular polarization (CP) antennas with high-frequency Gallium Arsenide (GaAs) Schottky diodes across the 10–20-GHz range. Our approach involves a systematic study of the rectifier's nonlinear behavior over wide frequency ranges, followed by the identification of an effective antenna candidate for co-design. This strategy effectively obviates the need for matching networks, filters, and extra components typically found in conventional wideband rectennas. Consequently, we present a co-design example: the proposed CP antenna, featuring a measured impedance bandwidth of 11.65–16.9 GHz (36.8%), a 3-dB axial ratio bandwidth (ARBW) of 12.55–16.9 GHz (29.54%), and a measured peak gain of 8.5 dBic. This design integrates CP magneto-electric (ME)-dipole units with rectifier topologies. Measured results show an RF–DC efficiency of over 50% within the 11–14.6 GHz (28%) and 10–18 dBm power range, with a maximum conversion efficiency of 61%. This design approach holds broad applicability for all wideband rectennas, offering notable advantages in terms of simplicity, efficiency, and compactness.**

***Index Terms*—Circular polarization (CP), co-design, rectennas, wideband, wireless power transfer (WPT).**

Received 23 January 2025; accepted 13 March 2025. Date of publication 25 March 2025; date of current version 27 June 2025. This work was supported in part by the National Key Research and Development Program of China under Grant 2023YFE0107900; in part by the National Natural Science Foundation of China (NSFC) under Grant 62071306; and in part by the Shenzhen Science and Technology Program under Grant JCYJ20200109113601723, Grant JSGG20210420091805014, Grant JSGG20210802154203011, and Grant GJHZ20180418190529516. *(Corresponding authors: Chaoyun Song; Yejun He; Cheng Zhang.)*

Jiupei Shi, Chaoyun Song, Yejun He, Zhonghe Zhang, Jinyao Zhang, and Wenting Li are with the State Key Laboratory of Radio Frequency Heterogeneous Integration, Sino-British Antennas and Propagation Joint Laboratory of Ministry of Science and Technology of China, Guangdong Engineering Research Center of Base Station Antennas and Propagation, Shenzhen Key Laboratory of Antennas and Propagation, College of Electronics and Information Engineering, Shenzhen University, Shenzhen 518060, China (e-mail: jiupei_shi@163.com; chaoyun.song@kcl.ac.uk; heyejun@126.com; zzh422384683@163.com; jyzhang@szu.edu.cn; w.li@szu.edu.cn).

Cheng Zhang is with the Shanghai Institute of Optics and Fine Mechanics, Chinese Academy of Sciences, Shanghai 201800, China, and also with the Hangzhou Institute for Advanced Study, University of Chinese Academy of Sciences, Hangzhou 310024, China (e-mail: czhangseu@foxmail.com).

Yuchao Wang is with the School of Physics and Mechanics, Wuhan University of Technology, Wuhan 430070, China (e-mail: yuchao9629@whut.edu.cn).

Yi Huang is with the Department of Electrical Engineering and Electronics, University of Liverpool, L69 3BX Liverpool, U.K. (e-mail: huangyi@liverpool.ac.uk).

Digital Object Identifier 10.1109/JIOT.2025.3553958

I. Introduction

THE EXTENSIVE development of mobile communication has enriched the spectrum resources available in the environment. Utilizing radio frequency (RF) resources in space to convert them into electrical energy for device charging has become a hot research topic. This approach not only effectively leverages the excess RF resources in space but also addresses the cost issue associated with frequent battery replacement. Furthermore, it is challenging to continuously power some implantable, portable, and other devices with wires, and the development of wireless power transmission (WPT) has brought new solutions to these challenges. Rectennas are crucial components in the design of WPT systems, as they receive RF energy from free space and convert it into direct current (DC) power to charge devices. This technology is particularly impactful for Internet of Things (IoT) applications, where many devices, such as sensors, wearables, and medical implants, require reliable and continuous power without the inconvenience and cost of frequent battery replacements.

In IoT applications, WPT can significantly enhance device longevity and performance by providing a steady and sustainable power source [1], [2]. For instance, in smart home systems, various sensors and devices can be powered wirelessly, ensuring seamless operation and reducing maintenance. In healthcare, implantable medical devices can benefit from wireless power, eliminating the need for invasive surgeries to replace batteries. Additionally, industrial IoT applications can leverage wireless power to enhance the systems in challenging environments [3], [4], [5], [6].

The wideband rectenna demonstrates robustness to signal frequency variations due to its ability to operate over a wide frequency range. In comparison with single frequency rectennas, it exhibits the capability to capture a broader spectrum of RF energy, thereby enhancing energy harvesting (EH) efficiency. Furthermore, it facilitates simultaneous charging of devices operating in different frequency bands, leading to improved charging efficiency. Not only does the wideband rectenna obviate the need for multiple rectenna designs for different frequency bands, but it also contributes to cost reduction in the overall wireless energy transfer

system. There, in recent years, wideband rectennas have shown promising applications in WPT and frequency-scanning multinode tracking [7], [8], [9]. Within these applications, utilizing circular polarization (CP) transceivers can effectively mitigate polarization mismatches and power loss in far-field scenarios. However, the development of wideband CP rectennas above sub 6G bands remains limited, primarily due to challenges in efficiency, axial ratio, impedance matching, and the nonlinearity of Gallium Arsenide (GaAs) Schottky diodes across a broad spectrum, ranging from 10 to 20 GHz.

Compared with high-frequency rectennas, multiband and wideband low-input power rectennas operating at sub-6 GHz have been devised to meet the growing need for ambient EH from radio waves, benefit for applications like battery-less IoT sensors and self-sustaining low-power devices [10], [11], [12], [13], [14], [15], [16], [17], [18], [19]. In high-frequency ranges, however, rectennas face a significant challenge due to the loss associated with PCB microstrip lines. This makes it crucial to implement co-design strategies already realized in the low frequency for wideband rectennas design which can eliminate the need for separated impedance matching and filtering components and thereby enhance the overall efficiency [20], [21], [22], [23], [24]. However, the high-frequency GaAs diodes present distinctly different nonlinear impedance variations over a much broader frequency range compared to the low frequency [25], posing significant challenges in developing effective approaches for high frequency rectenna co-design. In [24], a miniaturized traveling wave antenna array is co-designed with a small rectifier to achieve stable DC output power. However, the bandwidth of this rectenna is limited to 8.3%, and the measured maximum RF–DC conversion efficiency is only 50%. In addition, as previously discussed, wideband, high-gain CP antennas/arrays are particularly suitable for WPT systems. Hence, various CP rectennas in the sub-6G-band have been proposed for WPT systems [26], [27], [28], [29], [30], [31]. In contrast, the above sub-6G counterpart still lacks sufficient research. Only a few CP rectennas have been realized in [32], [33], [34], [35], and [36]. For instance, [34] developed a CP substrate integrated waveguide (SIW) cavity-backed antenna array with a band range of 24.2–25.8 GHz, but only achieving a maximum measured conversion efficiency of 42%. CP antennas in the Ku band have been documented, but their integration with rectifier circuits remains unexplored, as indicated in [37], [38], [39], and [40]. Reference [38] describes a wideband CP antenna achieved through the use of cross dipoles and quadruple parasitic elements; however, the antenna's axial ratio bandwidth (ARBW) is limited to only 0.1%. A wideband CP antenna is effectively realized in [39] using an ME-dipole, but the resulting antenna structure is relatively large. While the performance of CP rectennas has been notably advanced in [33], [34], [35], and [36], these designs are typically characterized by large sizes, complex structures, or lower efficiencies. For instance, [33] employs a complex three-layer Fabry–Perot (FP) resonator antenna combined with a rectifier circuit for WPT. In [34], an SIW back-cavity CP antenna array is used to optimize CP performance; however, the associated rectifier circuit requires additional matching branches, further complicating the structure and increasing its size. In [35], WPT is effectively achieved in a dual-band configuration; however, the complex SIW antenna array significantly enlarges the rectenna's size. In [36], although a higher conversion efficiency is attained, the bandwidth for over 50% conversion efficiency is limited to only 2%, and the proposed CP metasurface antenna structure is notably complex. Consequently, there is a pressing need to develop design strategies that not only broaden the operating bandwidth of high-frequency rectennas but also simplify their structure, reduce their size, and enhance their RF-to-DC efficiency.

In this article, we introduce a simple structure, compact, high-efficiency, wideband CP rectenna, co-designed for 10-20 GHz. Specifically, we utilize CP ME-dipole as the antenna unit to adapt the impedance nonlinear variation of the high-frequency Schottky diode MA4E1317, eliminating the losses associated with wideband matching networks operating in the high-frequency band of 10–20 GHz. Consequently, our co-designed CP rectennas demonstrate state-of-the-art performance, including a measured wide impedance bandwidth of 33.4%, the measured RF–DC conversion efficiency of up to 61%, peak gain of approximately 8.5 dBic for the CP antenna, and a beamwidth exceeding 60°.

The remainder of this article is organized as follows. Section II details the structure, operating principle, and results of the proposed wideband CP antenna. Section III discusses the co-design and working principle of the wideband rectifier. Experimental validation of the designed rectenna is presented in Section IV. Finally, Section V provides a summary of this article.

II. CP Antenna Design For Rectenna Co-Design

A. Why Circular Polarization?

As an important part of the WPT system, the selection of the antenna type is extremely important. Linearly polarized (LP) receiving antennas typically impose stringent requirements on the transmitting antenna. In practical scenarios, electromagnetic wave propagation can lead to deflection of polarization direction through reflection and refraction. When the polarization direction of the LP receiving antenna deviates from that of the transmitting antenna, signal reception diminishes accordingly. However, for CP antennas, the received signal remains consistent regardless of the polarization direction of the transmit antenna. This characteristic effectively suppresses multipath interference and mitigates issues related to polarization mismatch. As a result, CP antennas are capable of providing a more stable DC output voltage [41]. The advantages of CP antennas become even more significant in IoT multinode charging applications. In these scenarios, multiple devices are often scattered over a wide area, each requiring reliable and consistent power delivery. CP antennas ensure that all devices, regardless of their orientation or position relative to the transmitting antenna, receive a consistent signal. This uniformity simplifies the design and deployment of WPT systems for IoT networks, as it reduces the need for precise alignment between transmitters and receivers [42], [43]. To clearly demonstrate the performance advantages of CP antennas compared to LP antennas, the performance comparison is listed in Table I [41], [44]. This table clearly illustrates the

TABLE I
COMPARISON OF PERFORMANCE OF CIRCULARLY POLARIZED AND LP ANTENNAS

Performance	CP Receivers	LP Receivers
Polarization characteristic	All polarization	Linear polarization
Multipath effect	Low	Significant
TX and RX alignments	No alignment is needed	Require precise alignment
Harvested DC	Relatively stable	Unstable
Application flexibility	High flexibility\ wide coverage	Low flexibility\ small coverage

superior performance of CP antennas in terms of maintaining consistent signal reception, reducing interference, and providing stable DC output voltage. These advantages make CP antennas a more reliable choice for WPT systems, particularly in environments where signal polarization can be affected by various factors. Dual-linearly polarized (Dual-LP) antennas typically require two separate input ports with high isolations. They also necessitate precise alignment of the polarization directions between the transmit and receive antennas to maintain efficiency, with any mismatch leading to significant reductions in receive efficiency. In contrast, the proposed CP antenna requires only one input port, which facilitates integrated design with the rectifier and supports the development of miniaturized rectennas. Furthermore, integrating a Dual-LP antenna with a rectifier circuit requires separate processing of the two polarized signals. This often necessitates dual-channel rectifying circuits or additional combiners, thus adding to the complexity of circuit design and fabrication. In high-frequency applications, a Dual-LP antenna typically needs at least two rectifiers, potentially enlarging the overall design and introducing additional losses. Therefore, for simplicity, integration ease, and reduced system complexity, a single-port CP antenna is chosen for this study. In IoT applications, where numerous devices may be deployed in diverse and dynamic environments, the reliability and simplicity offered by CP antennas can significantly enhance the efficiency and effectiveness of WPT. This leads to more robust and scalable IoT networks, capable of supporting a wide range of devices with minimal maintenance and configuration.

B. Antenna Configuration

ME-dipole antennas, enhanced with the integration of complementary source technology, have demonstrated effective CP, along with a wide impedance bandwidth and high gain. These features make them highly suitable for applications in the microwave bands, as evidenced in [45], [46], [47], [48], [49], and [50].

Song et al. [8] have introduced the use of complementary source technology to achieve broadband CP performance. However, the working principle of the antenna was not detailed, nor was its performance verified in real-world scenarios. To address these gaps, we have conducted further research within the satellite communication band and potential 5G communication bands. This research includes a detailed explanation of the antenna's design process and working principles, along with rigorous testing of the antenna's performance as a receiver. In addition, the frequency has been scaled down in order to compromise the tradeoffs between device size and power loss of propagation. The proposed designs for the wideband left-handed circular-polarized (LHCP) and right-handed circular-polarized (RHCP) dipole antennas are depicted in Fig. 1. This article specifically focuses on the RHCP antenna to elucidate the operating principles of these antennas. The 3-D view of this antenna is presented in Fig. 2. Rogers RT 5880 with $\varepsilon_r = 2.2$, $\tan\delta = 0.0009$ was adopted as the two substrates (substrate 1 and substrate 2) with different thicknesses. Two symmetrical metal patches are printed on the top layer of substrate 1, where a pair of metal patches is diagonally connected. 4×7 metalized vias are placed in substrate 1, and the diameter of their metal vias is 0.52 mm. The electric (E) and magnetic (M) dipoles of the antenna are composed of two pairs of symmetrical metal patches and a transverse slot, respectively. For feeding the antenna, a microstrip is printed on the underside of substrate 2, while a transverse slot is etched on the top of this substrate to excite the radiation structure. Slot feeding, in comparison to probe feeding, simplifies the complexity of the rectifier in system integration. Electromagnetic waves are coupled from the feed port to substrate 1 through the etched transverse slot in the middle, thereby exciting the E- and M-dipoles. The design and simulation of the proposed antenna were carried out using commercial software—CST Microwave Studio 2021. The thicknesses of PCB substrates 1 and 2 are 3.175 and 0.508 mm, respectively, and the copper layer is 0.036-mm thick. To minimize fabrication costs, the two substrates are produced separately and then assembled using nylon (plastic)

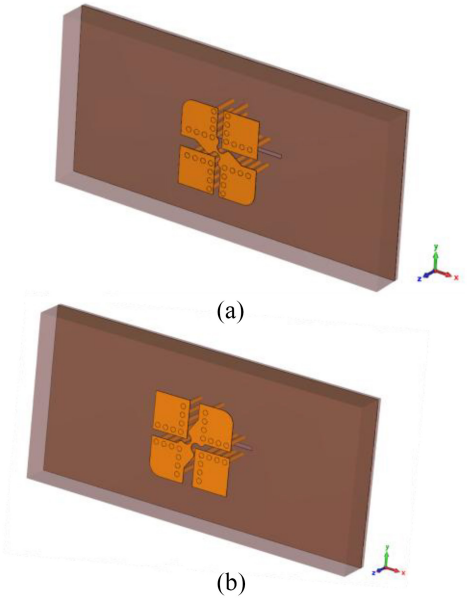

Fig. 1. Proposed wideband CP antenna. (a) LHCP. (b) RHCP.

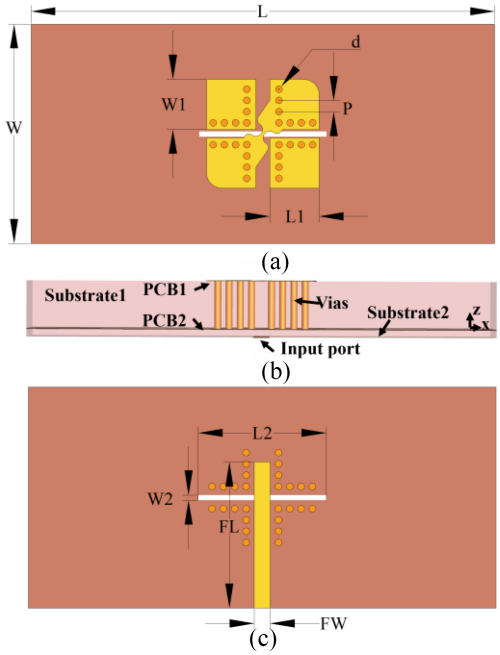

Fig. 2. Geometry of the proposed RHCP antenna. (a) Top view. (b) Side view. (c) Back view.

TABLE II
DIMENSIONS OF RHCP ANTENNA (UNIT: MM)

Parameters	Value	Parameters	Value
W	18	L_2	10.4
W_1	4.12	FL	11.9
W_2	0.4	FW	1.3
L	38	d	0.56
L_1	4.05	p	0.92

screws. The final optimized geometric dimensions of the proposed CP antenna are detailed in Table II.

C. Operating Principle of CP Radiation

The inclusion of a complementary source radiation in the antenna design introduces an additional resonant point, which serves to broaden the impedance bandwidth and enhance impedance matching within the operating band. As illustrated in Fig. 2, this configuration consists of four rectangular patches (two of which have one corner shaped into an arc), a metal strip with two circular arcs removed, and a pattern of 4×7 metalized vias. The four rectangular patches in conjunction with the transverse slot function as an E-dipole and an M-dipole, respectively. For CP, it is necessary to have two orthogonal LP modes of equal amplitude and a phase difference. Following the complementary sources concept, when the E-dipole and M-dipole are aligned parallel to each other, they can generate two orthogonal electric field components [45]. However, in this design, the transverse slot can only excite vertical E-dipole and parallel M-dipole, which together form LP ME-dipole [41]. To achieve CP, it is essential to excite another LP ME-dipole mode in the orthogonal direction. To this end, we incorporate a metal strip with removed circular arcs, which connects two of the rectangular patches, each having a corner in the shape of a circular arc. Based on the above ideas, the proposed ME-dipole antenna can well achieve wideband CP radiation. According to the concept of complementary sources, an E-dipole and an M-dipole with the same amplitude and phase difference, which are parallel to each other, can obtain two orthogonal electric field components [51], [52], [53]. The directions of the E- and M-dipoles are assumed to be along the direction, where the M-dipole can be regarded as a small ring antenna with area A_0 and its plane is perpendicular to the M-dipole. The far field of the E-dipole and the far field of the M-dipole can be expressed as follows [54]:

$$E_x = j\frac{60\pi \mathrm{I}}{r}\frac{L}{\lambda}\sin\theta e^{-jkr} \tag{1}$$

$$E_y = j\frac{120\pi^2 I}{r}\frac{A_0}{\lambda^2}\sin\theta e^{-jkr} \tag{2}$$

where L is the length of the E-dipole, I is the current, r is the radiation distance, and λ is the wavelength in free space. Therefore, when the E-dipole parallel to each other are excited with the same amplitude as the M-dipole, E_x and E_y have a phase difference. Furthermore, the values of E_x and E_y mainly depend on L and A_0, respectively. By adjusting the parameters to make the values of E_x and E_y equal, CP radiation is realized. The surface current distribution of the proposed CP antenna at 14.5 GHz is shown in Fig. 3, with RHCP as an example, to explain the operation of the antenna. At t = 0 and t = T/2, where T is the period of the oscillation, the surface currents on the four patches are mainly distributed along the diagonal direction, which indicates that the E-dipole in the diagonal direction is excited, and the amplitude of the current is sinusoidal distribution along this direction. At the same time, M-dipole along the diagonal direction is also excited. Similarly, at t = T/4 and t = 3T/4, the surface current on the patch is mainly distributed along the direction, where the E-dipole in this direction is excited at the same time as the M-dipole. The ME-dipole in these two directions is excited with a time delay of T/4, which corresponds to a phase difference equal to 90°. Therefore, CP radiation of this design is realized.

D. Antenna Performance

In order to verify the performance of the antenna, the antenna was fabricated, and the prototype of the fabricated antenna is shown in Fig. 4(a) and (b). Simulation and measurement of reflection coefficient $|S_{11}|$ is shown in Fig. 4(c). The results show that the proposed antenna can be used at 11.91–17.12 GHz ($|S_{11}| < -10$ dB) with a simulated wide impedance bandwidth of 35.9%. The measured fractional impedance bandwidth is 36.8%, which covers 11.65–16.9 GHz ($|S_{11}| < -10$ dB). Fig. 4(d) shows the measured and simulated 3-dB ARBW and gain results of the proposed antenna. It is shown that the simulated 3-dB ARBW of the proposed antenna ranges from 12.6 to 16.63 GHz, and 27.6% of the wide ARBW is achieved. The measured 3-dB ARBW ranges from 12.55 to

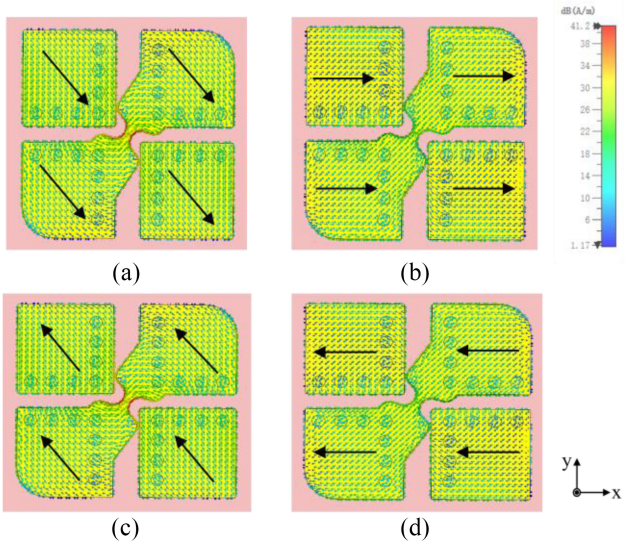

Fig. 3. Current distribution at 14.5 GHz of the proposed CP antenna at (a) $t = 0$, (b) $t = T/4$, (c) $t = T/2$, and (d) $t = 3T/4$.

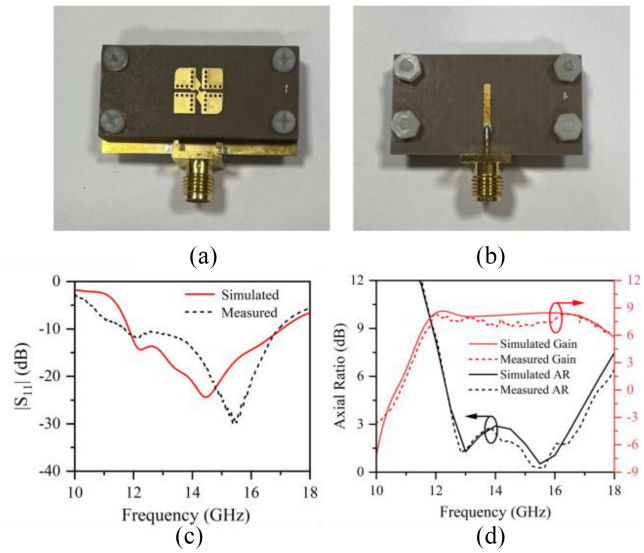

Fig. 4. Proposed CP ME-dipole antenna. (a) Top view of fabricated prototype. (b) Back view of fabricated prototype. (c) Simulated and measured $|S_{11}|$. (d) Simulated and measured AR and gain.

16.9 GHz (29.54%). Moreover, the band of the 3-dB axis ratio is in the impedance bandwidth, the overlap bandwidth reaches 29.54%, so it has a significant advantage in the wideband utilization. The simulated and measured peak gain of the proposed antenna is 8.7 and 8.5 dBic, respectively. Fig. 5 plots the simulated and measured radiation patterns for the CP antenna at 12.5, 14.5, and 16.5 GHz with $\varphi = 0^\circ$ and $\varphi = 90^\circ$. As shown in the figure, the measured results of the radiation pattern are generally consistent with the simulated results. The cross-polarization level is less than –15 dB, and the half-power beam bandwidth (HPBW) of this antenna is more than 60°. As the effective aperture of an antenna, which is a function of its gain, is proportional to the power it can harvest. Conversely, the beam width is related to spatial coverage, crucial for capturing power from wider incident angles. To balance the

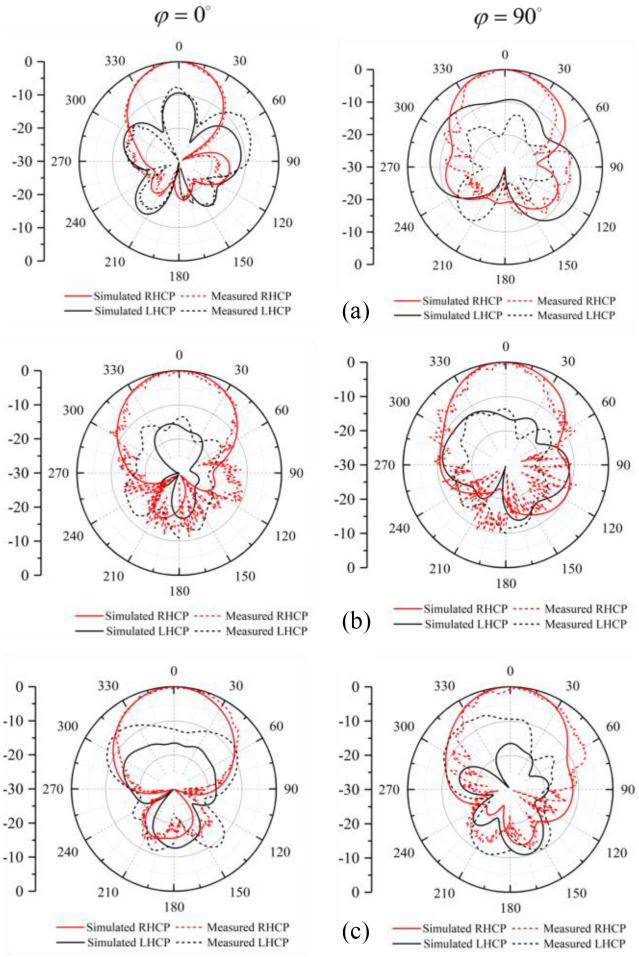

Fig. 5. Simulated and measured radiation patterns in $\varphi = 0^\circ$ and $\varphi = 90^\circ$ at (a) 12.5 GHz, (b) 14.5 GHz, and (c) 16.5 GHz.

tradeoffs between high gain and wide beam, we have chosen the ME-dipole antenna as the receiver due to its excellent combination of relatively wide beamwidth and high gain.

It can be observed from the results in Fig. 5 that the radiation pattern is distorted. The primary cause of this distortion is the inclusion of an SMA connector in the CST simulation of the CP antenna. Specifically, during the simulation process, both the CP antenna and the SMA connector are simulated together. The proximity of the SMA to the side of the antenna generates electromagnetic waves that lead to asymmetric radiation of the proposed CP antenna. The resulting pattern is illustrated in Fig. 6. The discrepancy between the simulated and measured results can be attributed to errors between fabrication, measurement, and alignment of the measuring device. The above results show that the antenna in this frequency band has the characteristics of low impedance bandwidth, high gain, wide HPBW, and wide 3-dB ARBW. Therefore, the proposed CP ME-dipole antenna based on complementary source technology operates in 10–20 GHz, which verifies the correctness of the proposed structure theory, and the structure has good radiation performance. Table III presents a performance comparison between our proposed CP antenna and other CP antennas previously reported in the literature. Although previous efforts

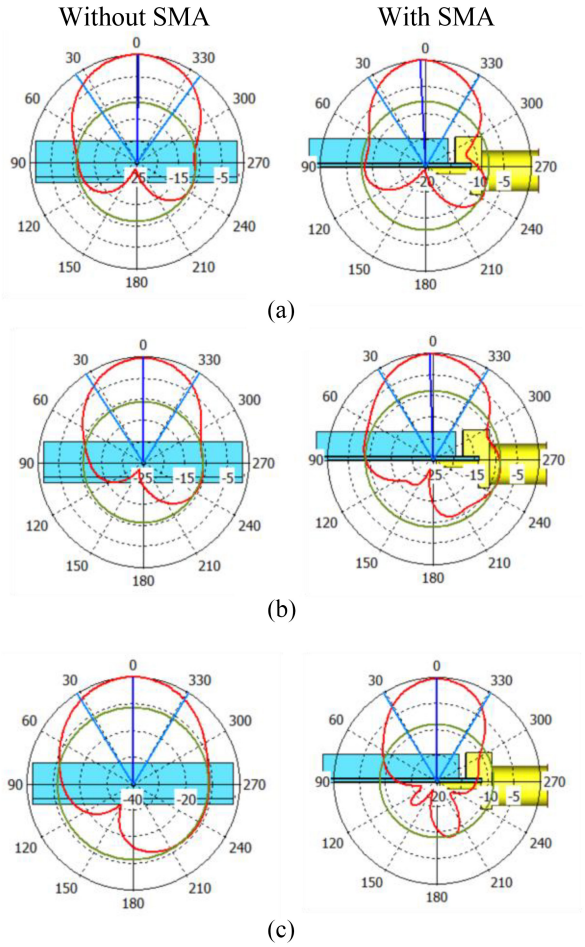

Fig. 6. Radiation pattern at $\varphi = 90^{\circ}$ for CP antenna with and without SMA in CST simulation. (a) 12.5 GHz. (b) 14.5 GHz. (c) 16.5 GHz.

have demonstrated good performance, they also exhibit some drawbacks. References [33] and [34] attempted to enhance the gain and impedance bandwidth of CP antennas using frequency-selective surface (FSS) coverage and by integrating slots on the patch, respectively. However, their 3-dB ARBW is restricted to only 10%. Similarly, the 3-dB ARBW for the antennas in [37] and [39] is also limited to less than 10%. In [37] and [38], cross dipole and ME-dipole antennas are employed to achieve a wider impedance bandwidth, respectively. Yet, these designs rely on coaxial feeders, complicating the integration with planar rectifier circuits and necessitating connections via 50-Ω SMA connectors. This approach not only increases the rectenna's overall size but also escalates costs. In [40], a dielectric resonator antenna was proposed, which achieved a better impedance bandwidth of more than 50%, but it had a narrow 3-dB ARBW and a low gain of only about 6 dBic in the operating band. The stacked antenna approach in [55] sees a 20% improvement in 3-dB ARBW. However, its multilayer structure adds to the complexity and manufacturing costs. In [32], the impedance bandwidth of a CP antenna is enhanced using an ME-dipole antenna with complementary source technology, but this bandwidth remains below 30%. Additionally, the use of SIW for feeding further complicates the overall antenna structure. In contrast

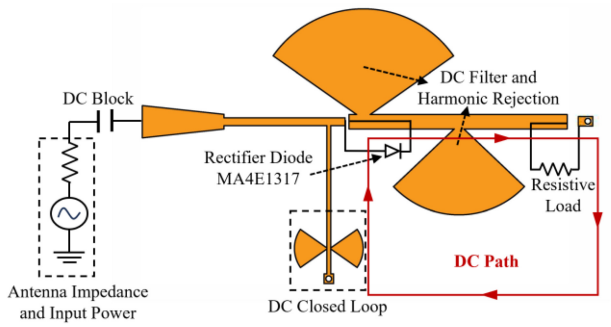

Fig. 7. Layout of the proposed rectifier.

to these reported designs, our proposed antenna offers several advantages, including a simpler structure, a wider impedance bandwidth, an expanded 3-dB ARBW, and a broad overlap bandwidth.

III. Co-Design Wideband Rectifying Circuit

The integration of a high-efficiency, wideband rectifier with the proposed wideband CP antenna is key to realizing the wideband characteristics of the overall system. The layout of the rectifier is depicted in Fig. 7. This structure is printed on a Rogers RT 5880 substrate with a thickness of 0.508 mm. The circuit model primarily consists of a shunt circuit, a high-frequency rectifier diode, a DC pass filter (fan-shaped stub), and a load resistor. The main topology features a DC filter placed in front of the load resistor, serving as an output filter. This filter can substitute the bypass capacitor, not only suppressing the second and third harmonics but also smoothing the voltage ripple at the DC output. This design enhances harmonic suppression, resulting in a rectification process characterized by minimal distortion and low loss. The overall design of the rectifier is relatively straightforward, eliminating the need for an additional impedance matching network. The feed port employs a conical line to facilitate the transmission of wideband impedance in the real part. A shunt circuit, positioned between the antenna and the diode, completes the DC closed loop. Functioning effectively as an inductance, its impact on impedance matching is minimal. The parameters of the ME-dipole antenna are fine-tuned to adjust the antenna impedance. Consequently, the impedance of the rectifier dynamically aligns with the antenna's impedance, ultimately achieving optimal conjugate matching within the operating band.

The selection of the rectifier diode is crucial in the overall performance of the rectifier circuit. In this study, we utilize GaAs Flip Chip Schottky Barrier Diodes, specifically the MA4E1317 model, which are capable of operating at frequencies up to 80 GHz [57]. These diodes are particularly well suited for rectifier designs that require a broad range of power and frequency.

To accurately represent the performance of the MA4E1317 diode, we use its equivalent model parameters. These parameters are extracted from the measurements of current–voltage (I–V), capacitance–voltage (C–V), and small-signal S parameters. This approach enhances the consistency between the

TABLE III
COMPARISON BETWEEN THE PROPOSED ANTENNA AND OTHER WIDEBAND CP ANTENNA

Ref.	Year	No. of Layer	Antenna type	Frequency (GHz)	RLBW (%)	ARBW (%)	PG (dBic)	Is it measured?	Size (λ_0^3)
[32]	2023	2	Complementary antenna	33.87-43.15	25.7	24.8	10.33	No	1.156*1.136*0.267
[33]	2016	3	FP metasurface antenna	33.6-37	10	6.5	17	Yes	3.7*3.7*0.2
[34]	2014	2	SIW cavity-backed antenna	24.2-25.8	6.4	4.5	10.3	Yes	2.5*2.5*0.085
[37]	2023	1	Crossed dipole antenna	15.5-23	38.9	0.1	NA	Yes	0.68*0.68*0.22
[38]	2023	2	ME-dipole antenna	9.26-13.14	34.6	34.6	NA	No	2.33*2.33*0.09
[39]	2021	1	Hybrid choke antenna	14.68-15.39	4.7	0.6	10.2	No	1.8*1.8*0.054
[40]	2024	1	Dielectric resonator antenna	8.26-14	51.57	11.01	8.1	Yes	0.68*0.68*0.096
[55]	2018	3	Stacked patch antenna	25-32.6	25.5	17.5	≈11.5	No	1.78*1.72*0.1
[56]	2018	2	Microstrip antenna	39.2-50.4	24.9	17.3	≈8.5	No	1.72*1.72*0.15
This Work	**2024**	**2**	**ME-dipole antenna**	**11.65-16.9**	**36.8**	**29.54**	**8.5**	**Yes**	**1.3*1.83*0.15**

RLBW: -10 dB Return loss bandwidth. ARBW: 3 dB axial ratio bandwidth. PG: peak gain.

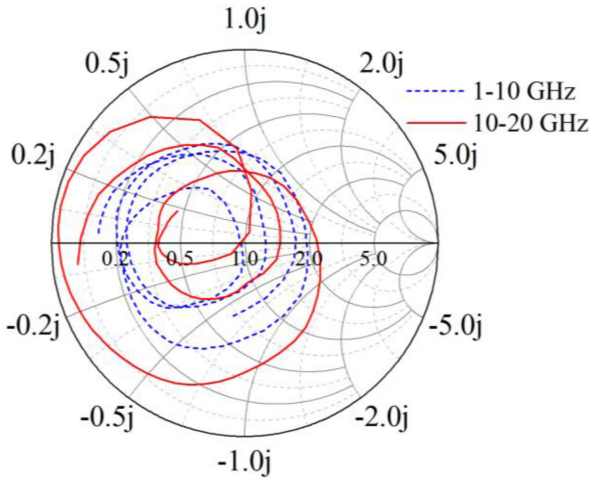

Fig. 8. Simulated impedance characteristic variation of the diode in the low frequency and high frequency.

diode's behavior in the designed circuit and its performance during testing [58]. The MA4E1317 diode offers low loss and high conversion efficiency, attributed to its small series resistance (4 Ω) and low zero-bias junction capacitance (0.02 PF). Furthermore, its high reverse breakdown voltage (7 V) ensures robustness against breakdown at high input power.

In order to analyze the impedance variation of the MA4E1317 diode, the impedance characteristic variation of the diode (the load resistance was set to the optimal value of 100 Ω) in the low-frequency band (1–10 GHz) and the high-frequency band (10–20 GHz) was simulated in the ADS, and the results are shown in the smith impedance variation circle chart of Fig. 8. The resulting figure shows that the high-frequency GaAs diode MA4E1317 exhibits significantly different nonlinear impedance variations over a wider frequency range compared with the low-frequency selection, which poses a significant challenge for the high band antenna co-design method. At the same time, we changed the input power value of the rectifier when the frequency was maintained at 10–20 GHz, and obtained the impedance change characteristics of the diode under different input powers (see Fig. 9). It can be seen from the figure that the impedance of the diode changes with the power value, and its nonlinear characteristics are also affected. Therefore, according to the effective reference data provided by the impedance variation curve, we use the co-design method to realize the conjugate matching between the CP antenna and the rectifying circuit in the wide frequency range from 10 to 20 GHz.

An important design feature of this rectifier is the inclusion of two metalized vias, serving the shunt circuit branch and the DC terminal grounding, respectively. The rectifier's structure is

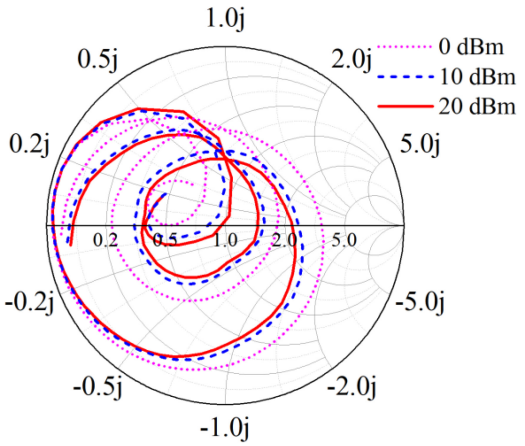

Fig. 9. Simulated impedance changes characteristics of the rectifier diode under different input powers.

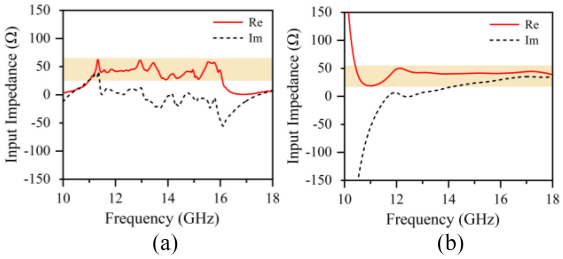

Fig. 10. Simulated input impedance. (a) Rectifier. (b) CP ME-dipole antenna.

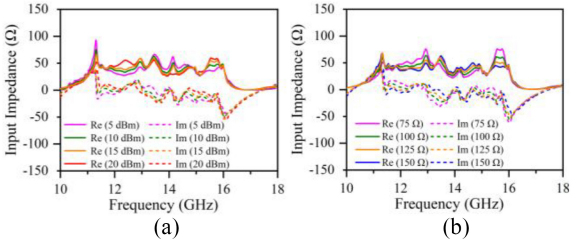

Fig. 11. Simulated impedance changes of the input port of the rectifier. (a) Different power values. (b) Different load values.

almost entirely solder-free, with soldering limited to the diodes and load resistors. This design choice effectively minimizes the adverse effects commonly associated with impedance matching networks and multiple solder joints.

The RF–DC conversion efficiency (η_r) of the rectifier can be calculated using the following formula:

$$\eta_r = \frac{\frac{V_{\mathrm{DC}}^2}{R_{\mathrm{Load}}}}{P_{\mathrm{in}}} \times 100\% \tag{3}$$

where V_{DC} is the DC voltage output at both ends of the load, R_{Load} is the load resistance, and P_{in} is the input power of the rectifier. Finally, the feed port of the antenna is connected to the rectifying circuit input port for co-simulation.

CST and ADS software are used to co-simulate the antenna and rectifier. The impedance values of the receive antennas are extracted using CST and the SNP file is exported, which is then imported into ADS for co-simulation to describe the overall conjugate matching process. This process can approximate the integration of the receiving antenna and the

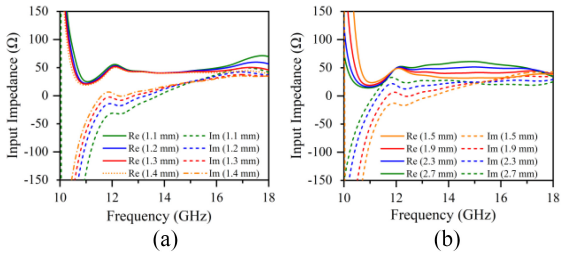

Fig. 12. Simulated impedance changes of the input port of CP ME-antenna. (a) Different *FW* values. (b) Different *FL* values.

rectifier, and the conjugate matching process can make the receiving antenna match the rectifier with the minimum loss. In detail, the input impedance of the final optimized CP ME-dipole antenna and rectifier (see Fig. 10) is shown here. Fig. 10(a) illustrates a gradual transition of the imaginary part value of the port impedance from negative to positive, indicating a shift in the antenna impedance characteristics from capacitive to inductive. Fig. 10(b) correspondingly reflects the change of rectifier port impedance from inductive to capacitive. Next, we show the influence of different parameters on the impedance of the rectifier and CP antenna. Subsequently, we demonstrate how the conjugate matching of the antenna and the rectifier is achieved, as shown in Figs. 11 and 12. It can be seen from Fig. 11 that the rectifier input impedance will change with the input power and load resistance. The optimal conjugate matching between the rectifier and the CP antenna can be realized by adjusting the input power, the load resistance value, and the circuit structure. Fig. 12 also demonstrates the impact of varying *FW* and *FL* values on the impedance of the CP antenna. Finally, by optimizing the rectifier and antenna structure parameters, the optimal conjugate matching is achieved when the input power is 18 dBm, the load resistance is 100 Ω, $FW = 1.3$ mm, and $FL = 11.9$ mm. Moreover, we also analyze the surface current distribution of the CP magnetoelectric dipole antenna at 12 and 16 GHz, as shown in Fig. 13. The figure shows that the antenna transitions from capacitive to inductive behavior as the frequency increases [42]. This transition reflects the trend of antenna port impedance variation, which is consistent with Fig. 10(b). After conjugate matching with the rectifier, the impedance comparison between the receiver antenna and the rectifier at some specific frequency points is listed in Table IV. For instance, at 14 GHz, the port output impedance of the receive antenna is 40+j15.9 Ω, and the port input impedance of the rectifier circuit is 26.6−j2.1 Ω. At 16 GHz, the output impedance of the receive antenna's port is 40.8+j29.7 Ω, while the input impedance of the rectifier circuit's port is 40.6−j44.4 Ω. This data demonstrates that the co-designed approach employed in this work successfully achieves optimal conjugate matching in the operating band. The congruence between the impedances of the antenna and the rectifier at various frequencies ensures effective power transfer and enhanced system performance, which is a crucial aspect of the design's efficacy.

The reflection coefficient $|S_{11}|$ and RF–DC conversion efficiency results of the final simulation of the rectenna after

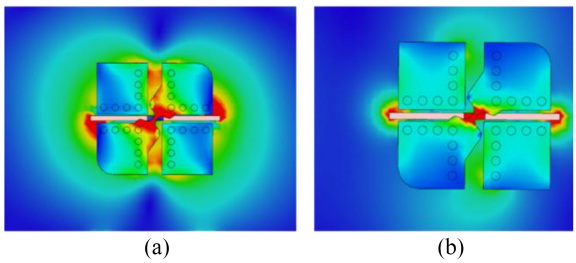

Fig. 13. Surface current distribution of the proposed CP ME-dipole antenna. (a) 12 GHz. (b) 16 GHz.

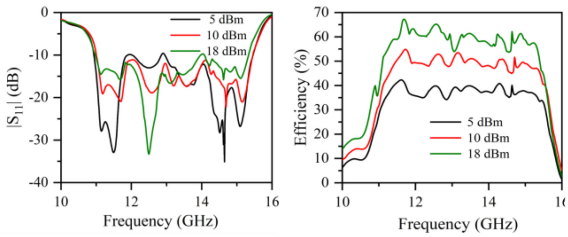

Fig. 14. Simulated (a) reflection coefficient and (b) RF-DC conversion efficiency at different power levels.

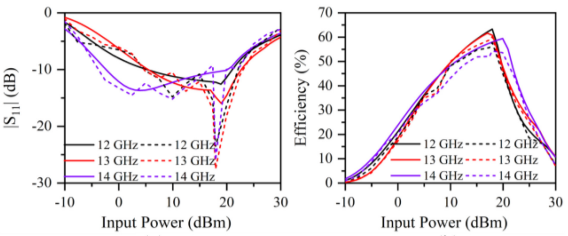

Fig. 15. Simulated (solid line) and measured (dashed line) reflection coefficient and RF–DC conversion efficiency at different frequencies.

TABLE IV
SIMULATED INPUT IMPEDANCES

Freq	CP antenna	Rectifying circuit
12 GHz	46.4+j6.1 Ω	43.5+j3.3 Ω
13 GHz	42.3+j6.7 Ω	61.2+j11.3 Ω
14 GHz	40.0+j15.9 Ω	26.6-j2.1 Ω
15 GHz	41.2+j23.7 Ω	42.6-j6.9 Ω
16 GHz	40.8+j29.7 Ω	40.6-j44.4 Ω

ADS optimization are shown in Fig. 14. Note that here $|S_{11}|$ is calculated using the complex impedance of the receive antenna with the rectifier, not just the conventional 50 Ω. The frequency characteristics in the 10–16 GHz band show that the proposed rectenna has a good impedance matching from 11.05 to 15.4 GHz. Moreover, the simulated conversion efficiency is up to 67% when the input power is 18 dBm. When the input power in the operating band is 5, 10, and 18 dBm, the simulated conversion efficiency of the rectenna is 40%, 50%, and 60%, respectively. The conversion efficiency mentioned above is obtained when the load impedance is 100 Ω. We

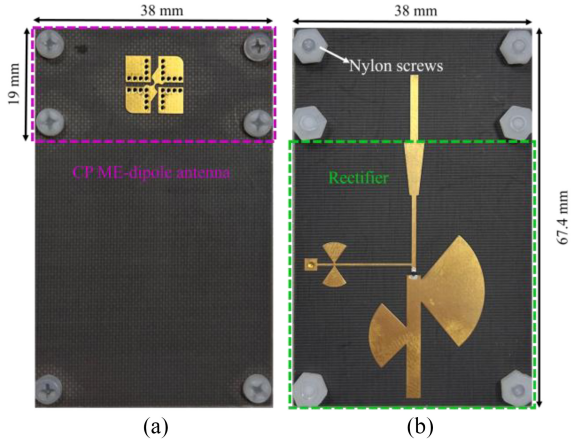

Fig. 16. Fabricated prototype of the proposed rectenna. (a) Top view. (b) Bottom view.

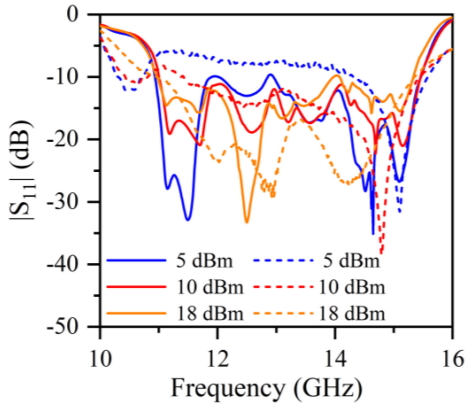

Fig. 17. Simulated (solid line) and measured (dashed line) reflection coefficient $|S_{11}|$ of rectifying circuit.

analyze the simulated and measured matching and RF–DC conversion efficiency for different input powers at 12, 13, and 14 GHz, respectively, as shown in Fig. 15(a) and (b). When the input power of the rectenna is in the range of −2∼22 dBm, the impedance matching $|S_{11}|$ is less than −10 dB. The maximum simulated efficiency of the rectenna ranges from 50% to 67% when the input power is around 18 dBm at different frequencies. The conversion efficiency is close to 0 for an input power of −10 dBm. The measurement results are consistent with the simulation results. In conclusion, the impedance bandwidth of the proposed wideband rectenna covers the frequency band of 11.05–15.4 GHz ($|S_{11}| < -10$ dB), the fractional bandwidth is 32.3%, and the simulated conversion efficiency in the operating band is greater than 50% (at an input power of 18 dBm). Moreover, the conversion efficiency is 30%–67% for input power of 5–18 dBm.

IV. FABRICATION AND MEASUREMENT OF RECTENNA

To test the performance of the proposed rectenna, the structure was fabricated using PCB technology as shown in Fig. 16. The purple marked in the figure is the proposed ME-dipole antenna with dimensions of 19×38×3.175 mm^3. Green indicates the rectifier, whose size is 38×67.4×0.508 mm^3 and is located on the top of the lower substrate. The feed port is connected to the feed line of the ME-dipole, and the

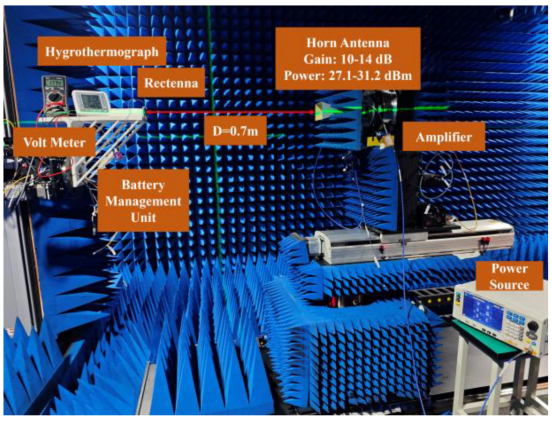

Fig. 18. OAT test of the wirelessly powered IoT sensors using the proposed rectenna inside an anechoic chamber.

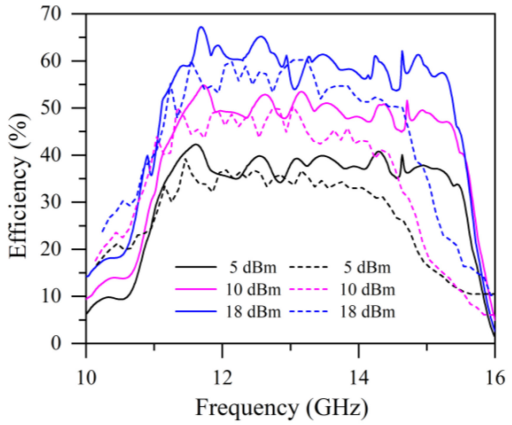

Fig. 19. Measured and simulated results of the proposed rectenna, solid lines represent simulation values and dashed lines represent test values: RF–DC conversion efficiency versus frequency under the input power of 5, 10, and 18 dBm.

position does not interfere with the CP ME-dipole antenna in the overlapping region. The two-layer PCB substrate does not require soldering or bonding. Six air holes are drilled along the edge of the substrate, and nylon screws are employed to secure it in place. To verify the impedance matching of the rectifier, the rectifier was tested independently, and its feed port was matched to a standard impedance of 50 Ω. The results of its simulated and measured reflection coefficient $|S_{11}|$ are shown in Fig. 17. According to the results in the figure, when the input power is 18 dBm, the reflection coefficient $|S_{11}|$ in the frequency band is better than –15 dB, which has a good impedance matching. Therefore, the correctness of the proposed rectifier structure is verified.

Next, to show the overall performance, we test the overall conversion efficiency of the rectenna. The experimental measurements setup of the rectenna system are displayed in Fig. 18. The entire system was evaluated in an anechoic chamber to ensure accurate and interference-free measurements. For the testing procedure, a signal generator, the Ceyer 1435D, was employed to generate RF signals within the range of 10–18 GHz. These RF signals were then amplified using Ceyear 80230F (0.5–40 GHz) broadband power amplifier. The signal is then transmitted through a 6–18 GHz horn antenna (HD-6018DRHA10S) with a gain of G_t, which radiates power of P_t. The proposed rectenna with gain G_r is at distance D from the transmit antenna to receive the transmitted signal, where the broadside direction of the circularly polarized dipole is aligned with the horn, and the value of distance D is 0.7 m. The load of the rectenna is connected to a BQ25504 dc–dc battery management unit (at the load resistor), which is used to stabilize the voltage output of the rectenna. The output port is connected to a thermohygrometer, which can display temperature and humidity values. The test process includes signal source sending signal to the transmitting antenna (horn antenna), rectenna harvesting energy from the horn antenna, and then converting RF energy into DC power through the rectifier, and then using the battery management unit to stabilize the voltage, and finally the thermohygrometer is displayed to successfully demonstrate the EH ability of the proposed rectenna. The received power of a rectenna can be expressed by the following formula:

$$P_r = P_t + G_t + G_r + 20\log_{10}\left(\frac{\lambda}{4\pi D}\right) \tag{4}$$

where P_r is the input RF power of the rectenna, P_t is the transmit power of the horn antenna, G_t is the realized gain of the horn antenna, G_r is the realized gain of the rectenna, λ is the wavelength in free space, and D is the transmission distance between the transmit antenna and the receive antenna.

Fig. 19 presents both measured and simulated results for the RF–DC conversion efficiency of the rectenna at different received powers, specifically at 5, 10, and 18 dBm. This figure demonstrates that the rectenna exhibits high RF–DC conversion efficiency within the targeted frequency band. The measured conversion efficiency is higher than 50% in the frequency band of 11–14.6 GHz, and the highest measured conversion efficiency can be as high as 61%. The consistency between the measured results and the simulated ones is notable, suggesting the effectiveness of the design and simulation process. However, some deviation between these results is observed, which may be attributed to factors, such as the soldering quality between the rectifier diode and the SMA joint, or discrepancies in the SPICE model of the rectifier diode and other components used in manufacturing and simulation. These discrepancies can lead to device mismatch and reduced conversion efficiency. Additionally, at low input powers, the diode may not operate in its optimal mode, resulting in a decrease in efficiency. Therefore, in order to improve this deviation, more accurate diode SPICE models can be explored, SMA joints that do not require welding and have low losses can be selected, and the use of connecting wires can be minimized during testing.

Table V compares the performance of our proposed rectenna with similar designs from existing literature. This comparison underscores that our rectenna achieves a broad impedance bandwidth and significantly enhanced conversion efficiency across an extensive frequency range. Notably, the measured conversion efficiency for more than 50% of the frequency fractional bandwidth reaches 28%, markedly surpassing the high conversion efficiency bandwidths reported in other studies. The work referenced in [34] is primarily focused on matching the antenna and circuit to 50 ohms at a single

TABLE V
COMPARISON BETWEEN THE PROPOSED RECTENNA AND OTHER WORKS

Ref.	Year	Frequency (GHz)	RLBW (%)	Overall complexity	Need impedance matching	Size (λ_0^3)	Measured efficiency > 50%	Maximum measured efficiency
[6]	2024	24.6-40	47.6	Complex	Yes	10.75*10.75*8.28	25-37.5 GHz	60%@6 dBm
[24]	2024	11.5-12.5	8.3	Complex	Yes	NA	≈12-12.5 GHz (4%)	≈50%@10 dBm
[33]	2016	34-36	5.7	Complex	Yes	5.62*4.29*0.15	34.1-34.3 GHz, 34.5-34.8 GHz (0.58%, 0.86%)	63.8% @18.9 dBm
[34]	2014	24.2-25.8	6.4	Complex	Yes	4.58*3.75*0.12	No	42% @12.6 dBm
[35]	2024	23.7-24.2 27.7-28.2	2.1/1.8	Complex	Yes	1.9*3.8*0.08	No	49.1/47.8%@ 18 dBm
[36]	2023	21-27.7	27.9	Complex	Yes	1.6*1.6*0.06	24-24.5 GHz (2%)	63%@15.2 dBm
[58]	2020	33-38	14	Complex	Yes	NA	NA	67% @19 dBm
This work	**2024**	**10.95-15.23**	**33.4**	**Simple**	**No**	**1.65*2.94*0.16**	**11-14.6 GHz (28%)**	**61% @18 dBm**

RLBW: –10 dB Return loss bandwidth. NA: Not available.

frequency of 24 GHz before integrating them. This approach introduces numerous matching branches at the circuit end, increasing both the complexity of the rectifier circuit and the physical size of the rectenna.

In contrast, our design targets wider bandwidths and non-50-Ω matching, resulting in a much simpler circuit structure than that described in [34]. Additionally, this article details the use of low-loss substrates and advanced integration methods that not only significantly improve conversion efficiency but also compact the overall structure of the rectenna, making it more suitable for IoT applications. Furthermore, compared to LP receiving antennas, the CP receiving antenna in our design more effectively addresses issues of multipath distortion and polarization mismatch.

Ultimately, this design maintains a simple structure and high conversion efficiency while keeping a low profile, providing a distinct advantage over rectenna designs that rely on antenna arrays.

V. CONCLUSION

In this article, we propose a co-design strategy for a wideband CP, simple structure and high-efficiency rectenna operating at 10–20-GHz frequencies. The rectenna integrates a wideband CP ME-dipole antenna and a wideband rectifier, achieving CP through a metal strip that generates two LP ME-dipole modes with a phase difference. Complementary source technology further enhances the antenna's bandwidth, resulting in a measured impedance bandwidth of 36.8% (11.65–16.9 GHz), a 3-dB ARBW of 29.54% (12.55–16.9 GHz), and a peak gain of 8.5 dBic. The rectenna also exhibits a wide measured impedance bandwidth of 33.4% (11.05–15.4 GHz) and a peak RF–DC conversion efficiency of 61%. This design eliminates the need for separate impedance matching circuits, ensuring excellent impedance matching and mitigating issues like multipath distortion and polarization mismatch. The rectenna's wide bandwidth, simple structure, compact, high efficiency, and broad beam make it ideal for IoT applications, such as powering smart home sensors, implantable medical devices, industrial IoT sensors, and wearable technology, enhancing performance and scalability in diverse and dynamic environments.

REFERENCES

[1] J. Kim and B. Clerckx, "Wireless information and power transfer for IoT: Pulse position modulation, integrated receiver, and experimental validation," *IEEE Internet Things J.*, vol. 9, no. 14, pp. 12378–12394, Jul. 2022.

[2] M. Wagih, G. S. Hilton, A. S. Weddell, and S. Beeby, "Millimeter-wave power transmission for compact and large-area wearable IoT devices based on a higher order mode wearable antenna," *IEEE Internet Things J.*, vol. 9, no. 7, pp. 5229–5239, Apr. 2022.

[3] G. Verma and V. Sharma, "A novel RF energy harvester for event-based environmental monitoring in wireless sensor networks," *IEEE Internet Things J.*, vol. 9, no. 5, pp. 3189–3203, Mar. 2022.

[4] Z. Liu, P. Wu, and G. Li, "A multibeam and surface plasmonic clothing with RF energy-localized harvester for powering battery-free wireless sensor," *IEEE Internet Things J.*, vol. 9, no. 15, pp. 13955–13964, Aug. 2022.

[5] Y. Wang et al., "Highly efficient broadband ambient energy harvesting system enhanced by meta-lens for wirelessly powering battery-less IoT devices," *IEEE Internet Things J.*, vol. 11, no. 16, pp. 26916–26928, Aug. 2024.

[6] F. Deng and K. M. Luk, "A broadband high-gain multibeam ambient millimeter-wave energy-harvesting system," *IEEE Internet Things J.*, vol. 11, no. 3, pp. 4888–4898, Feb. 2024.

[7] C. Song, L. Wang, Z. Chen, G. Goussetis, G. A. E. Vandenbosch, and Y. Huang, "Wideband mmWave wireless power transfer: Theory, design and experiments," in *Proc. EuCAP*, 2023, pp. 1–5.

[8] C. Song, L. Wang, M. Wagih, M. Poveda-Garcìa, and Y. Huang, "Novel mmWave wireless power transfer systems using broadband circularly polarized rectennas and leaky wave transmitters," in *Proc. USNC-URSI*, Portland, OR, USA, 2023, pp. 539–540.

[9] M. Wagih and C. Song, "mmWave wireless power transmission to flexible rectennas in absorptive and reflective media," in *Proc. USNC-URSI*, Portland, OR, USA, 2023, pp. 675–676.

[10] A. Tabesh and L. G. Frechette, "A low-power stand-alone adaptive circuit for harvesting energy from a piezoelectric micropower generator," *IEEE Trans. Ind. Electron.*, vol. 57, no. 3, pp. 840–849, Mar. 2010.

[11] C. Song, Y. Huang, J. Zhou, and P. Carter, "Improved ultrawideband rectennas using hybrid resistance compression technique," *IEEE Trans. Antennas Propag.*, vol. 65, no. 4, pp. 2057–2062, Apr. 2017.

[12] S. Yu, H. Liu, and L. Li, "Design of near-field focused metasurface for high-efficient wireless power transfer with multifocus characteristics," *IEEE Trans. Ind. Electron.*, vol. 66, no. 5, pp. 3993–4002, May 2019.

[13] L. Li, X. Zhang, C. Song, and Y. Huang, "Progress, challenges, and perspective on metasurfaces for ambient radio frequency energy harvesting," *Appl. Phys. Lett.*, vol. 116, no. 6, pp. 1–7, Feb. 2020.

[14] S. D. Joseph, Y. Huang, S. S. H. Hsu, A. Alieldin, and C. Song, "Second harmonic exploitation for high-efficiency wireless power transfer using duplexing rectenna," *IEEE Trans. Microw. Theory Techn.*, vol. 69, no. 1, pp. 482–494, Jan. 2021.

[15] C. Song et al., "A novel quartz clock with integrated wireless energy harvesting and sensing functions," *IEEE Trans. Ind. Electron.*, vol. 66, no. 5, pp. 4042–4053, May 2019.

[16] P. Lu, C. Song, and K. M. Huang, "Ultra-wideband rectenna using complementary resonant structure for microwave power transmission and energy harvesting," *IEEE Trans. Microw. Theory Techn.*, vol. 69, no. 7, pp. 3452–3462, Jul. 2021.

[17] Z. Chen et al., "Wearable rectenna with integrated miniaturized feeding slot and rectifier structure," *IEEE Trans. Antennas Propag.*, vol. 71, no. 5, pp. 3868–3881, May 2023.

[18] S. Lu, M. Böttigheimer, and N. Parspour, "An impedance mapping-based T-compensation network and control strategy for WPT system with full-bridge active rectifier," *IEEE Trans. Power Electron.*, vol. 71, no. 5, pp. 1–14, Jul. 2023.

[19] A. Eid, J. G. D. Hester, and M. M. Tentzeris, "5G as a wireless power grid," *Sci. Rep.*, vol. 11, no. 1, pp. 1–9, Dec. 2021.

[20] Y. Wang, X.-X. Yang, G.-N. Tan, and S. Gao, "Study on millimeter-wave SIW rectenna and arrays with high conversion efficiency," *IEEE Trans. Antennas Propag.*, vol. 69, no. 9, pp. 5503–5511, Sep. 2021.

[21] C. Song et al., "Matching network elimination in broadband rectennas for high-efficiency wireless power transfer and energy harvesting," *IEEE Trans. Ind. Electron.*, vol. 64, no. 5, pp. 3950–3961, May 2017.

[22] C. Song, Y. Huang, P. Carter, J. Zhou, S. D. Joseph, and G. Li, "Novel compact and broadband frequency-selectable rectennas for a wide input-Power and load impedance range," *IEEE Trans. Antennas Propag.*, vol. 66, no. 7, pp. 3306–3316, Jul. 2018.

[23] C. Cao, X. Zhang, C. Song, A. Georgiadis, and G. Goussetis, "A highly integrated multipolarization wideband rectenna for simultaneous wireless information and power transfer (SWIPT)," *IEEE Trans. Antennas Propag.*, vol. 71, no. 10, pp. 7980–7991, Oct. 2023.

[24] T. D. Ha, X. Nie, H. Bağcı, D. Erricolo, and P.-Y. Chen, "A low-profile, wide-angle, and bandwidth enhanced rectenna for radiative energy harvesting in the 12 GHz band," *IEEE Antennas Wireless Propag. Lett.*, vol. 23, pp. 3807–3811, 2024.

[25] C. Song et al., "Highly efficient wideband mmWave rectennas for wireless power transfer system with low-cost multinode tracking capability," *IEEE Trans. Antennas Propag.*, vol. 71, no. 11, pp. 8773–8787, Nov. 2023.

[26] C. Liu, Y. Zhang, and X. Liu, "Circularly polarized implantable antenna for 915 MHz ISM-band far-field wireless power transmission," *IEEE Antennas Wireless Propag. Lett.*, vol. 17, pp. 373–376, 2018.

[27] Y. Yang et al., "A 5.8 GHz circularly polarized rectenna with harmonic suppression and rectenna array for wireless power transfer," *IEEE Antennas Wireless Propag. Lett.*, vol. 17, pp. 1276–1280, 2018.

[28] Y. Liu, K. Huang, Y. Yang, and B. Zhang, "A low-profile lightweight circularly polarized rectenna array based on coplanar waveguide," *IEEE Antennas Wireless Propag. Lett.*, vol. 17, pp. 1659–1663, 2018.

[29] W. Lin, R. W. Ziolkowski, and J. Huang, "Electrically small, low-profile, highly efficient, huygens dipole rectennas for wirelessly powering Internet-of-Things devices," *IEEE Trans. Antennas Propag.*, vol. 67, no. 6, pp. 3670–3679, Jun. 2019.

[30] P. D. Hilario Re, S. K. Podilchak, S. A. Rotenberg, G. Goussetis, and J. Lee, "Circularly polarized retrodirective antenna array for wireless power transmission," *IEEE Trans. Antennas Propag.*, vol. 68, no. 4, pp. 2743–2752, Apr. 2020.

[31] D. Surender, M. A. Halimi, and T. Khan, "Circularly polarized DR-rectenna for 5G and Wi-Fi bands RF energy harvesting in smart city applications," *IETE Techn. Rev.*, vol. 39, no. 4, pp. 880–893, May 2021.

[32] J. Sang, L. Qian, M. Li, J. Wang, and Z. Zhu, "A wideband and high-Gain circularly polarized antenna array for radio-frequency energy harvesting applications," *IEEE Trans. Antennas Propag.*, vol. 71, no. 6, pp. 4874–4887, Jun. 2023.

[33] H. Mei, X. X. Yang, B. Han, and G. Tan, "High-efficiency microstrip rectenna for microwave power transmission at Ka band with low cost," *IET Microw. Antennas Propag.*, vol. 10, no. 15, pp. 1648–1655, Dec. 2016.

[34] S. Ladan, A. B. Guntupalli, and K. Wu, "A high-efficiency 24 GHz rectenna development towards millimeter-wave energy harvesting and wireless power transmission," *IEEE Trans Circuits Syst. I, Reg. Papers*, vol. 61, no. 12, pp. 3358–3366, Dec. 2014.

[35] Y. Wang, H. Pan, and T.-T. Chan, "A dual-band dual-sense circularly polarized rectenna for millimeter-wave power transmission," *IEEE Trans. Antennas Propag.*, vol. 73, no. 1, pp. 96–107, Jan. 2025.

[36] W. Huang, J. Du, X.-X. Yang, W. Che, and S. Gao, "A novel 24 GHz circularly polarized metasurface rectenna," *IET Microw. Antennas Propag.*, vol. 17, no. 6, pp. 419–426, May 2023.

[37] W. Li, Y. Zhang, X. He, K. Chen, G. Jiang, and X. Yang, "A Ku/K-band wideband crossed dipole circularly polarized array with low profile," *Microw. Opt. Technol. Lett.*, vol. 65, no. 11, pp. 2926–2932, Nov. 2023.

[38] L. Xiang, F. Wu, Z.-W. Miao, Z. H. Jiang, C. Yu, and W. Hong, "A wideband circularly polarized magnetoelectric dipole transmitarray antenna based on element rotation techniques," *IEEE Trans. Antennas Propag.*, vol. 71, no. 8, pp. 6953–6958, Aug. 2023.

[39] A. J. Davuluri and S. Polepalli, "A high gain Ku band antenna with circular polarization using hybrid choke ring structure," *IETE J. Res.*, vol. 69, no. 8, pp. 5618–5627, Sep. 2023.

[40] S. Sahu, R. K. Baudh, M. S. Parihar, and V. D. Kumar, "A wide band circularly polarized euler spiral dielectric resonator antenna for X/Ku-band applications," *IETE J. Res.*, vol. 70, no. 9, pp. 7294–7301, Sep. 2024.

[41] S. C. Gao, Q. Luo, and F. Zhu, "Introduction to circularly polarized antennas," in *Circularly Polarized Antennas*. New York, NY, USA: Wiley/IEEE Press, 2014, pp. 1–28.

[42] W. Lin and R. W. Ziolkowski, "Electrically small Huygens CP rectenna with a driven loop element maximizes its wireless power transfer efficiency," *IEEE Trans. Antennas Propag.*, vol. 68, no. 1, pp. 540–545, Jan. 2020.

[43] V. Kaim, N. Singh, B. K. Kanaujia, L. Matekovits, K. P. Esselle, and K. Rambabu, "Multi-channel implantable cubic rectenna MIMO system with CP diversity in orthogonal space for enhanced wireless power transfer in biotelemetry," *IEEE Trans. Antennas Propag.*, vol. 71, no. 1, pp. 200–214, Jan. 2023.

[44] M. S. Braasch, "Multipath effects," in *Global Positioning System: Theory and Applications*. Reston, VA, USA: Amer. Inst. Aeronaut. Astronaut., 1996, pp. 547–568.

[45] X. Bai, S. Qu, and K. B. Ng, "Millimeter-wave cavity-backed patch slot dipole for circularly polarized radiation," *IEEE Antennas Wireless Propag. Lett.*, vol. 12, pp. 1355–1358, 2013.

[46] Z. Ji, G.-H. Sun, and H. Wong, "A wideband circularly polarized complementary antenna for millimeter-wave applications," *IEEE Trans. Antennas Propag.*, vol. 70, no. 4, pp. 2392–2400, Apr. 2022.

[47] M. Li and K.-M. Luk, "Wideband magneto-electric dipole antenna for 60-GHz millimeter-wave communications," *IEEE Trans. Antenna Propag.*, vol. 63, no. 7, pp. 3276–3279, Jul. 2015.

[48] Z. Li, J. Liu, and Y. Long, "A quasi-magnetic-electric circularly polarized antenna with wide bandwidth," *IEEE Antennas Wireless Propag. Lett.*, vol. 18, pp. 2145–2149, 2019.

[49] X. Ruan, S. W. Qu, Q. Zhu, K. B. Ng, and C. H. Chan, "A complementary circularly polarized antenna for 60-GHz applications," *IEEE Antennas Wireless Propag. Lett.*, vol. 16, pp. 1373–1376, 2017.

[50] K.-M. Luk and B. Wu, "The magnetoelectric dipole—A wideband antenna for base stations in mobile communications," *Proc. IEEE*, vol. 100, no. 7, pp. 2297–2307, Jul. 2012.

[51] Y. Li, C. Wang, and Y. X. Guo, "A Ka-band wideband dual-polarized magnetoelectric dipole antenna array on LTCC," *IEEE Trans. Antennas Propag.*, vol. 68, no. 6, pp. 4985–4990, Jun. 2020.

[52] Y. Li and K.-M. Luk, "60-GHz dual-polarized two-dimensionalswitch beam wideband antenna array of aperture-coupled magneto-electric dipoles," *IEEE Trans. Antennas Propag.*, vol. 64, no. 2, pp. 554–563, Feb. 2016.

[53] J. Cao, H. Wang, S. Mou, P. Soothar, and J. Zhou, "An air cavity-fed circularly polarized magneto-electric dipole antenna array with gap waveguide technology for mm-Wave applications," *IEEE Trans. Antennas Propag.*, vol. 67, no. 9, pp. 6211–6216, Sep. 2019.
[54] J. D. Kraus and R. J. Marhefka, *Antennas for all Applications*. New York, NY, USA: McGraw-Hill, 2002.
[55] H. Xu, J. Zhou, K. Zhou, Q. Wu, Z. Yu, and W. Hong, "Planar wide band circularly polarized cavity-backed stacked patch antenna array for millimeter-wave applications," *IEEE Trans. Antennas Propag.*, vol. 66, no. 10, pp. 5170–5179, Oct. 2018.
[56] Z. Gan, Z.-H. Tu, Z.-M. Xie, Q.-X. Chu, and Y. Yao, "Compact wideband circularly polarized microstrip antenna array for 45 GHz application," *IEEE Trans. Antennas Propag.*, vol. 66, no. 11, pp. 6388–6392, Nov. 2018.
[57] S.-P. Gao, W. Hu, H. Zhang, and Y. Guo, "Millimeter-wave rectifiers using proprietary schottky diodes: Diode modeling and rectifier analysis," in *Proc. Wireless Power Week (WPW)*, 2022, pp. 180–184.
[58] Q. Chen, X. Chen, H. Cai, and F. Chen, "A waveguide-fed 35-GHz rectifier with high conversion efficiency," *IEEE Microw. Wireless Compon. Lett.*, vol. 30, no. 3, pp. 296–299, Mar. 2020.

Jiupei Shi (Student Member, IEEE) received the B.S. degree in electronics science and technology and the M.S. degree in radio physics from Xinyang Normal University, Xinyang, China, in 2018 and 2022, respectively. She is currently pursuing the Ph.D. degree in information and communication engineering with Shenzhen University, Shenzhen, China.

Her research interests include mmWave antennas, RF energy harvesting, and wireless power transmission.

Chaoyun Song (Senior Member, IEEE) received the B.E., M.S., and Ph.D. degrees in electrical engineering and electronics from the University of Liverpool, Liverpool, U.K., in 2012, 2013, and 2017, respectively.

He is currently a Distinguished Professor with the State Key Laboratory of Radio Frequency Heterogeneous Integration, Shenzhen University, Shenzhen, China, and an Associate Professor (Senior Lecturer) with the Department of Engineering, King's College London, London, U.K. Prior to this, he was an Assistant Professor with the School of Engineering and Physical Sciences, Heriot-Watt University, Edinburgh, U.K. He has published more than 150 papers (including 59 IEEE TRANSACTIONS) in peer-reviewed journals and conference proceedings. His current research interests include wireless energy harvesting and power transfer, rectifying antennas (rectennas), flexible and stretchable electronics, metamaterials and meta-surface, and low-power sensors.

Dr. Song has been the recipient of numerous international awards, including the Inaugural Best Paper Award of the PROCEEDINGS OF THE IEEE, the IEEE AP-S Young Professional Ambassador 2023, the IEEE AP-S Raj Mittra Travel Grant 2023, the EuCAP 2023 Best Antenna Paper Award, the IET Innovation Award in 2018, and the BAE Systems Chairman's Award in 2017. He also has served as the Session Chair and/or TPC Member for various conferences, including EuCAP2018, IEEE AP-S Symposium 2021, IEEE VTC2022-fall, EuCAP2023, IEEE AP-S Symposium 2023, and EuCAP2024. He has consistently contributed as a Reviewer for esteemed journals, such as *Nature Electronics*, *Nature Communications*, *Advanced Materials*, *Advanced Functional Materials*, and *Nano Energy*, in addition to reviewing for over 15 IEEE TRANSACTIONS. He was a Top-200 reviewer for IEEE TRANSACTIONS ON ANTENNA AND PROPAGATION from 2021 to 2023. He has also taken on the role of Guest Editor of prestigious publications, including IEEE ANTENNAS AND WIRELESS PROPAGATION LETTERS, IEEE OPEN JOURNAL ON ANTENNAS AND PROPAGATION, and *IET Electronic Letters*.

Yejun He (Senior Member, IEEE) received the Ph.D. degree in information and communication engineering from Huazhong University of Science and Technology, Wuhan, China, in 2005.

From 2005 to 2006, he was a Research Associate with the Department of Electronic and Information Engineering, The Hong Kong Polytechnic University, Hong Kong. From 2006 to 2007, he was a Research Associate with the Department of Electronic Engineering, Faculty of Engineering, The Chinese University of Hong Kong, Hong Kong. In 2012, he joined the Department of Electrical and Computer Engineering, University of Waterloo, Waterloo, ON, Canada, as a Visiting Professor. From 2013 to 2015, he was an Advanced Visiting Scholar (Visiting Professor) with the School of Electrical and Computer Engineering, Georgia Institute of Technology, Atlanta, GA, USA. From 2023 to 2024, he was an Advanced Research Scholar (Visiting Professor) with the Department of Electrical and Computer Engineering, National University of Singapore, Singapore. Since 2006, he has been a Faculty Member with Shenzhen University, Shenzhen, China, where he is currently a Full Professor with the College of Electronics and Information Engineering, the Director of Sino-British Antennas and Propagation Joint Laboratory of Ministry of Science and Technology of the People's Republic of China, the Director of the Guangdong Engineering Research Center of Base Station Antennas and Propagation, and the Director of the Shenzhen Key Laboratory of Antennas and Propagation, Shenzhen, and the Chair of IEEE Antennas and Propagation Society-Shenzhen Chapter. He was selected as an "Expert with Special Government Allowance from the State Council in China," a Fellow of China Institute of Communications, a Leading Talent in the "Guangdong Special Support Program" in 2024, and the Shenzhen "Pengcheng Scholar" Distinguished Professor, China, in 2020, respectively. He has authored or co-authored more than 330 refereed journal and conference papers and seven books. He holds over 20 patents. He is the Principal Investigator for over 40 current or finished research projects, including the National Natural Science Foundation of China, the Science and Technology Program of Guangdong Province, and the Science and Technology Program of Shenzhen City. His research interests include wireless communications, antennas, and radio frequency.

Dr. He received the Shenzhen Overseas High-Caliber Personnel Level B (Peacock Plan Award B) and the Shenzhen High-Level Professional Talent (Local Leading Talent). He received the Second Prize of Guangdong Provincial Science and Technology Progress Award in 2023, the 10th Guangdong Provincial Patent Excellence Award in 2023, the Second Prize of Shenzhen Science and Technology Progress Award in 2017, and the Three Prize of Guangdong Provincial Science and Technology Progress Award in 2018. He also obtained the 2022 IEEE APS Outstanding Chapter Award. He is serving as an Associate Editor for IEEE TRANSACTIONS ON ANTENNAS AND PROPAGATION, IEEE TRANSACTIONS ON VEHICULAR TECHNOLOGY, IEEE TRANSACTIONS ON MOBILE COMPUTING, *IEEE Antennas and Propagation Magazine*, IEEE ANTENNAS AND WIRELESS PROPAGATION LETTERS, *International Journal of Communication Systems*, *China Communications*, and *ZTE Communications*. He has served as a reviewer for various journals, such as IEEE TRANSACTIONS ON VEHICULAR TECHNOLOGY, IEEE TRANSACTIONS ON COMMUNICATIONS, IEEE TRANSACTIONS ON INDUSTRIAL ELECTRONICS, IEEE TRANSACTIONS ON ANTENNAS AND PROPAGATION, IEEE WIRELESS COMMUNICATIONS, IEEE COMMUNICATIONS LETTERS, *International Journal of Communication Systems*, and *Wireless Personal Communications*. He has served as a Technical Program Committee Member or a Session Chair for various conferences, including the IEEE Global Telecommunications Conference (GLOBECOM), the IEEE International Conference on Communications (ICC), the IEEE Wireless Communication Networking Conference (WCNC), and the IEEE Vehicular Technology Conference (VTC). He served as the TPC Chair for IEEE ComComAp 2021 and the General Chair for IEEE ComComAp 2019. He was selected as a Board Member of the IEEE Wireless and Optical Communications Conference (WOCC). He acted as the Publicity Chair of several international conferences, such as the IEEE PIMRC 2012. He served as the TPC Co-Chair for WOCC 2023/2022/2019/2015, APCAP 2023, UCMMT 2023, ACES-China2023, and NEMO 2020 and the Executive Chair for 2024 IEEE International Workshop of Radio Frequency and Antenna Technologies (RFAT 2024). He is serving as an Executive Chair for 2025 IEEE International Workshop of Radio Frequency and Antenna Technologies (RFAT 2025). He is a Fellow of IET.

Cheng Zhang (Member, IEEE) was born in Henan, China. He received the M.S. degree in material science and technology from Wuhan University of Technology, Wuhan, China, in 2015, and the Ph.D degree from the State Key Laboratory of Millimeter Waves, Department of Radio Engineering, Southeast University, Nanjing, China, in 2019.

He is currently a Professor with Shanghai Institute of Optics and Fine Mechanics, Chinese Academy of Sciences, Shanghai, China. He has authored or co-authored more than 70 publications, including six highly cited papers, with citation over 2000 times. His current research interests are EM energy harvesting, stealth metamaterial/metasurface, and multiphysical manipulation.

Prof. Zhang was a recipient of the 2020 China Top-Cited Paper Award from IOP Publishing and the Top Articles in Device Physics for Applied Physics Letters (two papers). He received the Honor mention award for Best Student Paper Contest in 2018 IEEE International Workshop on Antenna Technology (iWAT) and the Appreciation Award of invited talk in 2018 IEEE International Conference on Computational Electromagnetics (ICCEM).

Yuchao Wang received the B.S. degree in electronic science and technology and the M.S. degree from Wuhan University of Technology, Wuhan, China, in 2018 and 2021, respectively.

His research interests include planar antennas, RF energy harvesting, and wireless power transmission.

Zhonghe Zhang (Graduate Student Member, IEEE) was born in Jinzhong, Shanxi, China, in 1995. He received the B.S. and M.E. degrees from North University of China, Taiyuan, China, in 2018 and 2021, respectively, and the Ph.D. degree from the College of Electronics and Information Engineering, Shenzhen University, Shenzhen, China, in 2024.

He is currently a Postdoctoral Researcher with Shenzhen University. His current research interests include millimeter wave antennas and arrays, reconfigurable antennas and arrays, and multibeam antennas and arrays.

Jinyao Zhang received the B.Eng. and Ph.D. degrees in electrical and electronic engineering from the University of Liverpool, Liverpool, U.K., in 2018 and 2023, respectively.

In early 2024, he joined the School of Electronic and Information Engineering, Shenzhen University, Shenzhen, China, as a Postdoctoral Researcher. His research focuses on wireless power transfer, microwave energy harvesting, simultaneous wireless information and power transfer, metasurface antenna, and rectenna design.

Wenting Li (Member, IEEE) received the B.S. degree in electronic information engineering and the M.S. degree in electromagnetic field and microwave technology from Northwestern Polytechnical University, Xi'an, China, in 2011 and 2014, respectively, and the Ph.D. degree in electronic engineering from the University of Kent, Canterbury, U.K., in 2019.

He is currently an Assistant Professor with the College of Electronics and Information Engineering, Shenzhen University, Shenzhen, China. His current research interests include reflect array antennas, reconfigurable antennas, circularly polarized antennas, and multibeam antennas.

Dr. Li is a recipient of the Shenzhen Overseas High-Caliber Personnel Level C ("Peacock Plan Award" C).

Yi Huang (Fellow, IEEE) received the B.Sc. degree in physics from Wuhan University, Wuhan, China, in 1984, the M.Sc.(Eng) degree in microwave engineering from Nanjing Research Institute of Electronics Technology (NRIET), Nanjing, China, in 1987, and the D.Phil. degree in communications from the University of Oxford, Oxford, U.K., in 1994.

Since 1987, he has been actively engaged in research on antennas, wireless communications, radar, EMC, and applied electromagnetics. More recently, his focus has expanded to include novel materials for antennas, wireless energy harvesting, and power transfer. His professional experience includes three years as a Radar Engineer with NRIET and research positions with the University of Birmingham, Birmingham, U.K., University of Oxford, Oxford, U.K., and University of Essex, Colchester, U.K. In 1994, he worked as a Research Fellow with British Telecom Labs before joining the Department of Electrical Engineering and Electronics, the University of Liverpool, Liverpool, U.K., in 1995. He is currently a Full Professor of Wireless Engineering and the Head of the High-Frequency Engineering Group. He has published over 500 peer-reviewed papers in leading international journals and conferences. He is the author of several books, including *Antennas: From Theory to Practice* (Wiley, 2008 and 2021) and *Reverberation Chambers* (Wiley, 2016 and 2019).

Prof. Huang's contributions have earned him over 10 prestigious awards, such as the IET Premium Award 2022 for Best Paper, the EuCAP 2023 Best Antenna Paper, the IET Innovation Award 2018, and the BAE Systems Chairman's Award 2017. He has secured numerous research grants from research councils, government agencies, charities, the EU, and industry and has acted as a consultant to various companies He has served on multiple national and international technical committees, including the IET, EPSRC, European ACE, COST-IC0603, COST-IC1102, and EurAAP. He has also held editorial roles for leading journals, serving as an Associate Editor and Guest Editor of four international journals, including IEEE ANTENNAS AND WIRELESS PROPAGATION LETTERS from 2016 to 2022, and as the Editor-in-Chief of *Wireless Engineering and Technology* from 2014 to 2023. He was the U.K./Ireland Delegate to EurAAP from 2016 to 2020 and has been a keynote/invited speaker and organizer of numerous international conferences and workshops, such as EuCAP, IEEE iWAT, WiCom, and LAPC. He is currently an Associate Editor of IEEE TRANSACTIONS ON ANTENNAS AND PROPAGATION, a College Member of EPSRC, a Member of the IEEE AP-S New Technology Directions Committee, and a Distinguished Lecturer of IEEE AP-S. He is a Senior Fellow of the Higher Education Academy (SFHEA). More information can be found from: https://www.liverpool.ac.uk/people/yi-huang.